Analysis of the actuation properties of charged multilayer films

Elshad Allahyarov, Hartmut Löwen, and Lei Zhu

Citation: Journal of Applied Physics **117**, 034504 (2015); doi: 10.1063/1.4906064
View online: http://dx.doi.org/10.1063/1.4906064
View Table of Contents: http://scitation.aip.org/content/aip/journal/jap/117/3?ver=pdfcov
Published by the AIP Publishing

Analysis of the actuation properties of charged multilayer films

Elshad Allahyarov,[1,2,3] Hartmut Löwen,[1] and Lei Zhu[3]
[1]*Institut für Theoretische Physik II: Weiche Materie, Heinrich-Heine Universität Düsseldorf Universitätstrasse 1, 40225 Düsseldorf, Germany*
[2]*Theoretical Department, Joint Institute for High Temperatures, Russian Academy of Sciences (IVTAN), 13/19 Izhorskaya street, Moscow 125412, Russia*
[3]*Department of Macromolecular Science and Engineering, Case Western Reserve University, Cleveland, Ohio 44106-7202, USA*

(Received 9 October 2014; accepted 5 January 2015; published online 15 January 2015)

Combining elasticity theory with electrostatics, we calculate the actuation response of a charged multilayer film, which is composed of consecutively stacked piezoelectric and polymeric elastomer layers, with respect to an applied voltage. Depending on the individual material properties and polarity of the applied voltage, we show that the composite multilayer can exhibit actuation properties which are considerably better than the response of the individual constituents. It is also shown that there is a window for applied voltages within which the thickness of the composite film expands, a condition that cannot be achieved in single layer films. In particular, we apply and evaluate our theory for various piezoelectric and dielectric elastomers. The results obtained will be helpful to develop tailored composite materials with specific actuation characteristics. © *2015 AIP Publishing LLC*. [http://dx.doi.org/10.1063/1.4906064]

I. INTRODUCTION

Active composite materials are a wide class of materials used in engineering, electronics, and transducer applications, such as hydrostatic hydrophones, acoustic sensors, medical and non-destructive testing transducers, and artificial muscles.[1–9] The actuation of such materials is provided by an electroactive polymer (EAP) component in their structure. Generally speaking, the EAP can be classified into two main categories: ionic electroactive polymers (IAP) and field active polymers (FAP).[3,10] IAP materials use electrically driven mass transport of ions and other charged species to obtain a shape change and vice-versa. The mostly used examples for such IAP are ionic polymers.[3] The main disadvantages of these materials are their slow strain relaxation due to the built-up pressure gradient, the necessity of their humidification, and, as a result, a restricted temperature regime for their operation.[3] Contrary to IAP materials, the actuation of FAP materials is based on polarization processes in the dielectrics, or, on the interaction between immobile charges and the applied field. Examples of such materials include most of dielectric elastomers[3,10–14] and porous polypropylene (PP) film electrets.[4,15] Because of the Coulomb nature of the interactions, the field activation in such polymers is fast, and most importantly, FAP are insensitive to temperature and humidity conditions.

Most of current FAP applications rely on using monolithic films sandwiched between metal electrodes. When polarized, a compressing Maxwellian pressure squeezes the polymer film. Thus, by changing the voltage between the electrodes, it is possible to regulate the strength of compressing force and achieve necessary deformations in the layer. Then, by assembling such monolithic Maxwell films into different structures, it is possible to enhance the actuator behavior of the multilayer. Another way to improve actuation properties of the FAP materials is based on the use of piezo-elastomer composite materials with sharp dielectric discontinuities.[3,14,16–19] Here, the film actuation gets additional enhancement from the interface polarization under applied voltages. The actuation can be further boosted if the interface is deliberately charged. Such charging has been employed in electrets, for example, in highly insulating polymer foam films, such as biaxially stretched PP foams.[14,20] In this case, additional charge separation appears on the opposing bubble surfaces, which creates huge permanent dipoles in the film. These dipoles strongly react to the external field generating additional intrafilm forces, which either swell or shrink the film. Assembling of charged PP foam films into a stack increases their piezoelectric coefficient from 600 pC/N to 2010 pC/N.[15]

Corona charging has been also used for inorganic electrets like SiO_2 and for SiO_2/Si_3N_4 multilayers, where a positive charge q is deposited at a depth d in the electret.[21] In order to detrap the bulk trapping sites, which are shallower in energy and have lower density than the interface trapping sites, the charged multilayer is annealed at higher temperatures. As shown in Ref. 22, the piezoelectric constant is large when the injected charges are close to interfaces rather than being in the bulk. Thin layers also inhibit partial diffusion of the interface charges into the bulk,[23] preventing the decrease in piezoelectric reaction constants.

The morphological structure of a composite material is usually described by means of the a-b connectivity factor,[1,24] where the a term describes the connectivity of the primary active phase, and the b term corresponds to the connectivity of the secondary passive phase. The simplest architecture for a piezo-polymer composite material is a layered material corresponding to a *2–2* connectivity with a flat interface between the layers. Such multilayer films have low density and fast actuation speed, and are best candidates for artificial muscle applications.[10] Other possible architectures include a

matrix elastomer polymer impregnated with piezoelectric fillers. In this case, the connectivity can be varied between *1–3* and *3–3*.[16,25]

In this study, we present a generalized theory for the actuation properties of charged multilayer films by combining elasticity theory with a phenomenological description of electrostatics. Our research broadens the study of Tuncer *et al.*[22] and Kacprzyk *et al.*[30,31] to the case of a multilayer film for which we carry out a systematic analysis of the piezoelectric charge (d_{33}) and voltage (g_{33}) coefficients under applied voltages and pressures. We consider a composite multilayer with a *2–2* connectivity, where one layer is an active piezoelectric layer and the second layer is a passive dielectric elastomer layer. Our aim is to find optimal elastic and dielectric coefficients for the hybrid material at which its actuation response is superior to the response of a single layer film. We show that the response coefficients of the composite material have very rich features compared to the individual constituents of the multilayer. For example, under suitable conditions, the composite is considerably squeezed than the individual material would do. We also show that there is a threshold voltage V_0 which defines a swelling window for the applied voltage $-V_0 < V < 0$ for the multilayer, when the composite swells. For a charged multilayer under an external voltage, we derive a full expression for the coefficient d_{33} showing its linear dependence on V. Transferring the multilayer deformation to its capacity of lifting a mass, we show that considered multilayers are several times more efficient than their single layer counterparts. The rest of the paper is organized as follows. We describe our system parameters in Sec. II. The general theory of multilayer actuation is given in Sec. III. Section IV is devoted to the calculation of actuation coefficients in linear perturbation theory. We discuss our results in Sec. V and conclude in Sec. VI.

II. SYSTEM SET-UP AND BASIC PARAMETERS

We consider a sandwich-like multilayer structure consisting of consecutively assembled dielectric layers *1* and *2* with

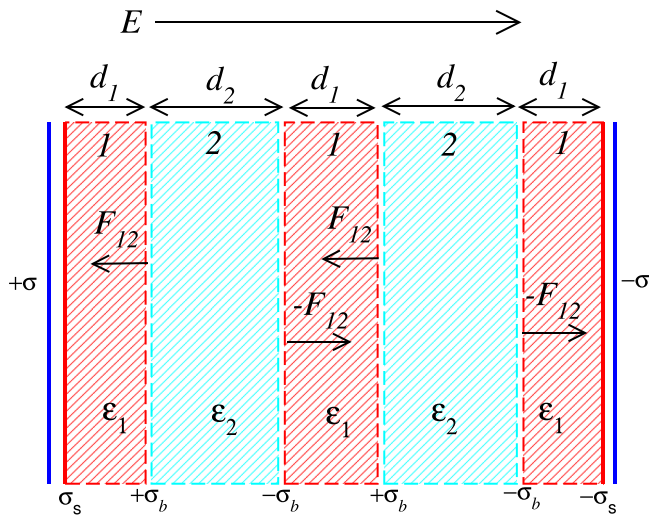

FIG. 1. Schematic picture of a multilayer ($2n-1=5$) with $n=3$ layers *1* of thickness d_1, and $n-1=2$ layers *2* of thickness d_2 under external electric field E. Also shown are interface forces $\pm F_{12}$, interface charges $\pm\sigma_b$, and surface charges $\pm\sigma_s$. The direction of interface forces are shown for multilayers with $\epsilon_1 > \epsilon_2$ from Table II.

TABLE I. Dielectric constants ϵ and Young modulus Y for the PZT, PVDF, Barex, VHB, and SEBS dielectrics.

Material	ϵ	Y [MPa]
PZT	3800	50 000
PVDF	12	3000
Barex	5.2	65
VHB	4.7	0.5
SEBS	2.0	1

dielectric permittivities ϵ_1 and ϵ_2. The multilayer in total has *2n-1* layers: n hard layers *1* of thickness d_1 and $(n-1)$ soft layers *2* of thickness d_2, see the schematic illustration in Figure 1. We assume that the layering is along the z direction, and along the xy direction, the multilayer has infinite dimensions.

For the layer *1*, we consider three different piezodielectric candidates: piezoelectric transducer (PZT), polyvinylidene fluoride (PVDF), and Barex (Barex 210 acrylonitrile-methyl acrylate copolymer). For the layer *2*, two different dielectric elastomers, Very High Bond acrylic foam tape (3M VHB™) and SEBS (styrene-(ethylene- *co*-butylene)-styrene triblock copolymer), are considered. The dielectric constants and Young's moduli of these materials are listed in Table I. For typical materials, such as multilayer films given in Table II, we will consider the case of $\epsilon_1 > \epsilon_2$ and $Y_1 > Y_2$.

We assume that all layers *1* were initially impregnated with free ions at elevated temperatures. Then applying a strong polarizing field, the charges of opposite signs are separated towards the layer boundaries. We assume that there are strong trapping centers at the *1–2* interface which block possible ion recombination when the poling field is removed and the membrane is cooled down to room temperature. Thus, after poling, the *1–2* interfaces possess bipolar $\pm\sigma_b$ surface charge densities, and the total charge of the film is zero. The interface charges will polarize neighboring layers *1* and *2*, which will in turn generate internal electrostatic forces acting on the interfaces. We assume that the charged film has been given enough time to relax to an equilibrium state where internal forces are fully balanced by the elastic forces of the deformed layers.

When a charged and equilibrated film is put under external voltage, both layers will be polarized and subsequently deformed. We disregard any deformation related structural changes in the polymer, as well as the altering of their dielectric and mechanical properties. For simplicity, fringe effects at the layer boundaries will be considered non-important. This will avoid mechanical instability problems on the layer interfaces, like wrinkling and buckling,[26–28] when the deformation rates of the layers do not match. For

TABLE II. A list of dielectric multilayer films with the ratios ϵ_1/ϵ_2, Y_1/Y_2, and the values for the threshold voltage V_0 given by Eq. (7) in the text.

Multilayer	ϵ_1/ϵ_2	Y_1/Y_2	V_0 (in volts)
PZT/VHB	810	10^5	2.98×10^3
PVDF/VHB	3	6×10^3	1.51×10^6
PVDF/SEBS	6	3×10^3	1.13×10^6
Barex/SEBS	3	7×10^2	3.53×10^6

all deformations, we will consider a constant volume condition explained in Appendix A. We consider a particular case when the interface on the left corner is charged positively, and the interface on the right corner is charged negatively. The applied voltage V can change its polarity from positive to negative values. Note that a negative voltage $V<0$ applied on the multilayer with positive $\sigma_b > 0$ on its left corner is qualitatively the same as applying a positive voltage $V>0$ on the multilayer with negative interface $\sigma_b < 0$ on its left corner.

In the Sec. III, we employ linear response theory to calculate local fields in the layers, and define the interface electrostatic pressure. These parameters are then used to analyze piezoelectric actuation properties of the films.

III. ACTUATION OF A CHARGED MULTILAYER UNDER EXTERNAL VOLTAGE *V*

The local fields E_i in the layers i ($i=1,2$) of the film can be found from the following two equations:

(i) Gauss law for the electric displacement $D_i = \epsilon_0\epsilon_i E_i$ across a surface carrying the free-charge surface density σ_b:

$$D_2 - D_1 = +\sigma_b. \tag{1}$$

(ii) Kirchhoff's voltage law for the potential drop across the film

$$V = nE_1d_1 + (n-1)E_2d_2 = \frac{D}{\epsilon_0\epsilon_1 n}d_1 + \frac{D}{\epsilon_0\epsilon_2(n-1)}d_2. \tag{2}$$

Thus, for the local fields, we get

$$E_1 = \frac{\epsilon_0\epsilon_2 V - \sigma_b(n-1)d_2}{\epsilon_0 A(\epsilon,n,d)}, \tag{3}$$

and

$$E_2 = \frac{\epsilon_0\epsilon_1 V + \sigma_b n d_1}{\epsilon_0 A(\epsilon,n,d)}, \tag{4}$$

where $A(\epsilon,n,d) = \epsilon_2 d_1 n + \epsilon_1 d_2(n-1)$. Note that under a short circuit condition $V=0$, fields E_1 and E_2 are directed in opposite directions and $E_1 = -\frac{n-1}{n}\frac{d_2}{d_1}E_2$. Also, a thinner layer is having a larger electric field in it.

The pressure on the interface *1–2* is defined as

$$p = D_2E_2 - D_1E_1. \tag{5}$$

Here, we assume a constant volume condition for deforming layers, which results in the doubling of the Maxwellian pressure, see Appendix A for more details. Maintaining a constant volume condition also means that lateral extensions of the layers will be different and thus cause nonlinear deformations mentioned in Sec. II. Using Eqs. (3) and (4), we arrive at

$$p = \frac{\epsilon_0\epsilon_1\epsilon_2 V^2(\epsilon_1-\epsilon_2)}{A^2(\epsilon,n,d)} + \frac{2\epsilon_1\epsilon_2 V\sigma_b L}{A^2(\epsilon,n,d)} + \frac{\epsilon_2 d_1^2 n^2 - \epsilon_1 d_2^2 (n-1)^2}{\epsilon_0 A^2(\epsilon,n,d)}\sigma_b^2. \tag{6}$$

Here, the first term has a quadratic dependence on V and corresponds to a polarization force. The second term is a linear function of V and σ_b, and thus describes the Coulomb interaction between a charged interface and electrodes. The last term with no dependence on V describes internal electrostatic forces between charged interfaces. This term, as already mentioned in Sec. II, is balanced by internal elastic forces of the film, and thus should be omitted from further consideration.

The sign of the pressure, sign(p), depends on the competition of the first two terms in Eq. (6). Whereas the first term is always positive, the second term can be either positive or negative depending on the sign of V. A positive sign of pressure p means that the force acting on the interface *1–2*, and defined as $\vec{F}_{12} = pS\vec{z}/2$, is directed from the material *1* to the material *2*. Here, S is the interface area. The force on the *2–1* interface is $\vec{F}_{21} = -\vec{F}_{12}$, thus under a positive pressure $p>0$, the layer *1* swells, whereas the layer *2* shrinks. Opposite deformations for the layers will take place for a negative pressure $p<0$.

For $V>0$ and $V<-V_0$, the total pressure in Eq. (6) is positive, whereas for $-V_0<V<0$, it is negative. The threshold potential V_0 is defined as

$$V_0 = \frac{2L\sigma_b}{\epsilon_0(\epsilon_1-\epsilon_2)}. \tag{7}$$

Maximal squeezing of the layer *1* happens at $V=-\frac{V_0}{2}$ under

$$p_{\max} = -\frac{\epsilon_1\epsilon_2}{\epsilon_0(\epsilon_1-\epsilon_2)}\left(\frac{\sigma_b L}{A(\epsilon,n,d)}\right)^2. \tag{8}$$

The applied voltage V changes the multilayer thickness from L to $L_{\text{new}} = L + \Delta L$, where $\Delta L = n\Delta d_1 + (n-1)\Delta d_2$, and individual layer deformations are

$$\Delta d_i = |p|\alpha_i d_i / Y_i \tag{9}$$

with their sign defined as

$$\alpha_i = (-1)^{i+1}\text{sign}(p). \tag{10}$$

The deformation of the boundary layers *1* facing the electrodes is different from the deformation of the inner layers *1*. This is because of the fact that boundary layers have only one interface *1–2*. On the other hand, for a multilayer with a large number of layers, a contribution from the two boundary layers to the total deformation of the film is small. Thus, for simplicity, we will assume that all layers *1*, including the boundary layers, experience the same deformation Δd_1 under the applied voltage V.

Using Eqs. (5) and (9), for the total multilayer deformation ΔL we get

$$\Delta L = \left|\frac{\epsilon_0\epsilon_1\epsilon_2 V^2}{A(\epsilon,n,d)^2}(\epsilon_1-\epsilon_2) + \frac{2\epsilon_1\epsilon_2 V\sigma_b L}{A(\epsilon,n,d)^2}\right| \times \left(\frac{n\alpha_1 d_1}{Y_1} + \frac{(n-1)\alpha_2 d_2}{Y_2}\right). \tag{11}$$

The most interesting case here is a positive value of ΔL, $\Delta L>0$, because a film swelling can never be achieved

in a single layer film. For $p>0$, a film swelling $\Delta L>0$ is possible when

$$\frac{d_1}{d_2}>\frac{n-1}{n}\frac{Y_1}{Y_2}, \quad \text{and} \quad V>0, \quad V<-V_0. \tag{12}$$

For $p<0$, a film swelling $\Delta L>0$ happens if

$$\frac{d_1}{d_2}<\frac{n-1}{n}\frac{Y_1}{Y_2}, \quad -V_0<V<0. \tag{13}$$

Because we assume $Y_1>Y_2$, and limit ourselves by cases $d_1/d_2<50$, a film swelling can be observed only when the conditions of Eq. (13) are met in composite materials listed in Table II. The film swelling comes from the expansion of the width of the elastomer layer.

IV. PIEZOELECTRIC VOLTAGE COEFFICIENT g_{33}

The material's suitability for sensing and actuation applications is usually based on the assessment of its piezoelectric coefficients g_{33} and d_{33}.[2–6,25] The g_{33} coefficient defines a multilayer strain resulting from an applied voltage V

$$g_{33}=\Sigma/|V|, \tag{14}$$

where the multilayer strain is

$$\Sigma=\Delta L/L, \tag{15}$$

and ΔL is given by expression Eq. (11).

Because we are interested in developing composite multilayers with actuation features superior to a single layer, it is advisable to calculate the relative piezoelectric coefficient g_{33}^R:

$$g_{33}^R=g_{33}/g_{33}^S=\Sigma/\Sigma_S, \tag{16}$$

where

$$g_{33}^S=\Sigma_S/|V|=-\epsilon_0\epsilon_2|V|/(L^2Y_2) \tag{17}$$

is a piezoelectric coefficient for a single layer film of a thickness L made from material 2, see Appendix B for details. Equation (16) can be written as

$$g_{33}^R=-\left|\frac{\epsilon_1(\epsilon_1-\epsilon_2)LY_2}{A(\epsilon,n,d)^2}+\frac{2\epsilon_1\sigma_bL^2Y_2}{A(\epsilon,n,d)^2\epsilon_0V}\right|\left(\frac{n\alpha_1d_1}{Y_1}+\frac{(n-1)\alpha_2d_2}{Y_2}\right). \tag{18}$$

Similar to ΔL, the most interesting case here is $-g_{33}^R>0$, meaning a swelling of the multilayer. When $-g_{33}^R<-1$, the multilayer will be shrunken more efficiently than a single layer film.

V. ACTUATION COEFFICIENT d_{33}

The d_{33} piezoelectric coefficient measures the induced electric field at the multilayer surface generated by the applied P. This is a main mechanism harbored in the microphone applications.[29] The field at the film surface E_1 is related to the film surface charge density σ_s, see Eq. (19) below. Therefore, we will focus on the change $\Delta\sigma_s$ instead of the change ΔE_1. We assume that a fixed voltage V is provided from an external source, such as a capacitor, and the initial film thickness L_0 and surface charge σ_0 have relaxed to their equilibrium values L and σ_s as a response to V. The surface charge σ_s is defined as

$$\sigma_s=\epsilon_0\epsilon_1E_1-\frac{\epsilon_0V}{L}. \tag{19}$$

Replacing E_1 by Eq. (3), we get

$$\sigma_s=\frac{\epsilon_0\epsilon_1\epsilon_2V}{A(\epsilon,n,d)}-\frac{\epsilon_1d_2\sigma_b(n-1)}{A(\epsilon,n,d)}-\frac{\epsilon_0V}{L}. \tag{20}$$

Note that the sign of the surface charge changes from negative to positive at $V=V_1$:

$$V_1=\frac{\epsilon_1d_2\sigma_b(n-1)}{\epsilon_1\epsilon_2-\frac{A(\epsilon,n,d)}{L}}, \tag{21}$$

where V_1 is always positive provided $\sigma_b>0$.

The change of the surface charge $\Delta\sigma_s$ under the applied pressure P is associated with the layer deformations $\Delta d_i=d_iP/Y_i$,

$$\Delta\sigma_s=\frac{\partial\sigma_s}{\partial d_1}d_1\frac{\Delta d_1}{d_1}+\frac{\partial\sigma_s}{\partial d_2}d_2\frac{\Delta d_2}{d_2}. \tag{22}$$

This expression, using Eqs. (20) and (9), can be rewritten as

$$d_{33}=\frac{\Delta\sigma_s}{P}=\frac{\epsilon_1\epsilon_2n(n-1)d_1d_2\sigma_b}{A^2(\epsilon,n,d)}\left(\frac{1}{Y_1}-\frac{1}{Y_2}\right)+\Phi(V), \tag{23}$$

where $\Phi(V)$ is a linear function of V

$$\frac{\Phi(V)}{V}=-\frac{\epsilon_0\epsilon_1\epsilon_2n}{A^2(\epsilon,n,d)}\sum\frac{d_i\epsilon_j}{Y_i}+\frac{\epsilon_0}{L^2}\sum\frac{d_i}{Y_i}-\frac{\epsilon_0d_2}{Y_2}\left(\frac{1}{L^2}+\frac{\epsilon_1^2\epsilon_2}{A^2(\epsilon,n,d)}\right). \tag{24}$$

It is evident that d_{33} has two separate contributions: the first contribution comes from the interface charge density σ_b and the second contribution is associated with V. For a particular case of a double layer with $V=0$, the first term coincides with the expression given in Refs. 22, 30, and 31. Also, the first term in Eq. (23) is completely negative for $Y_1>Y_2$ considered in this paper. Hence, under a decompressing pressure $P>0$ (a pressure under which the film swells in z direction, $L_{new}>L$) and no external field V, $\Delta\sigma_s<0$, which means that any film expansion in z direction in this simple case will result in the decrease in the absolute value of σ_s. Note that $\Delta\sigma_s$ is directly related to the change of the surface potential.

For the comparison of multilayer actuation with the actuation of a single layer, we calculate the relative piezoelectric coefficient

$$d_{33}^R=d_{33}/d_{33}^S. \tag{25}$$

Here, the single layer coefficient d_{33}^S can be derived from Eq. (24) by using $d_1 = 0$, $d_2 = L$, $\epsilon_1 = \epsilon_2$, and $Y_1 = Y_2$,

$$d_{33}^S = -\frac{\epsilon_0 |V|}{L Y_2}(\epsilon_2 - 1). \tag{26}$$

The final expression for d_{33}^R is

$$d_{33}^R = d_{33}^I + d_{33}^{II} + d_{33}^{III}, \tag{27}$$

where d_{33}^I and d_{33}^{II} have no dependence on V and σ_s,

$$d_{33}^I = -\frac{\text{sign}(V)}{\epsilon_2 - 1}\frac{1}{L}\left(n d_1 \frac{Y_2}{Y_1} + (n-1)d_2\right), \tag{28}$$

$$d_{33}^{II} = \frac{\epsilon_1 \epsilon_2 \text{sign}(V)}{\epsilon_2 - 1}\frac{L}{A^2(\epsilon, n, d)}\left(n d_1 \epsilon_2 \frac{Y_2}{Y_1} + (n-1)d_2 \epsilon_1\right). \tag{29}$$

These two terms have opposite contributions to the relative coefficient d_{33}^R. For example, at positive voltages $V > 0$, the d_{33}^I term is negative and thus contributes to the increase in $\sigma_s(P)$ when the film is expanded in z direction. However, for the same potential, positive d_{33}^{II} results in the decreasing in $\sigma_s(P)$ when the film is expanded in z direction. The third part of d_{33}^R,

$$d_{33}^{III} = \frac{\epsilon_1 \epsilon_2}{\epsilon_0(\epsilon_2 - 1)}\frac{L}{A^2(\epsilon, n, d)} n(n-1) d_1 d_2 \left(1 - \frac{Y_2}{Y_1}\right)\frac{\sigma_b}{|V|}, \tag{30}$$

which depends both on σ_s and V, is always positive, $d_{33}^{III} > 0$, because the following conditions $\sigma_b > 0$ and $Y_1 > Y_2$ were assumed in our setup. Again, similar to the Sec. IV, the most interesting case here is when the total coefficient is positive, $-d_{33}^R > 0$, when the surface charge density $\sigma_s(P)$ increases under a decompressing $P > 0$, or, equivalently, when $\sigma_s(P)$ decreases under a compressing $P < 0$ (a pressure under which the film shrinks in z direction, $L_{new} < L$). Another interesting case is $-d_{33}^R < -1$, which corresponds to a better actuation of the multilayer compared to the actuation of a single layer film.

VI. RESULTS

Local electric fields in layers *1* and *2* of the PZT-VHB multilayer film according to Eqs. (3) and (4) are shown in Figure 2 as a function of the number of layers *1*. First, as it is expected, the layer *2* with a smaller dielectric constant ϵ_2 has a larger electric field in it. Second, with the increase in n, both fields decrease, however the rescaled field $E_2 L/V$ is always above the single layer field $EL/V = 1$. The decrease in E_i $(i = 1, 2)$ is related to the fact that the derivative $(E_i)_n'$ is $\left(\frac{E_i}{E}\right)_n' \approx -\frac{1}{n^2}$, thus $E_i/E \approx 1/n$.

Film strains from Eq. (15) for four different composites listed in Table II are shown in Figure 3. Our analytical results are given for $L = 5000\,\mu$m, $\sigma_b = 0.01$ C/m^2, and for three thickness ratios $d = d_1/d_2 = 0.1, 1, 10$. The applied voltage is varied between $-2V_0$ and $2V_0$, and the values of V_0 are given in Table II. The multilayer has in total $2n - 1 = 39$, from which $n = 20$ are piezoelectric layers *1*,

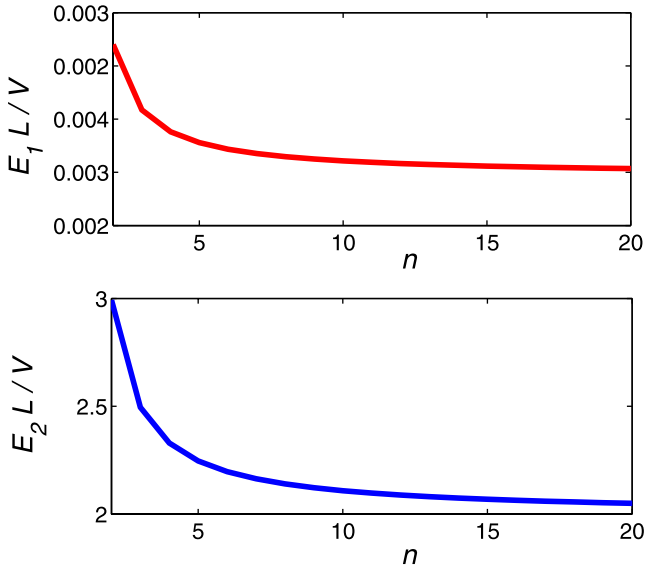

FIG. 2. Normalized by V/L local fields E_i (see Eqs. (3) and (4) in the text) in the layers $i = 1$ (above) and $i = 2$ (below) as a function of the layer number n calculated for the PST-VHB film with L = 5000 μm, $\sigma_s = 0.0$ C/m^2, $d_1 = d_2$, and $V = 1000$ V.

and $n - 1 = 19$ are elastomer layers *2*. As it seen from Figure 3, the multilayer strain is positive in the $-V_0 < V < 0$ window. The strain has a maximal swelling at $V = -V_0/2$. A higher swelling is expected for larger values of V_0. For all other voltages V, the multilayer shrinks, similar to a single layer behavior, which is shown as a black dashed line in Figure 3. If the thickness of the piezolayer becomes much larger than the thickness of the elastomer, which is the case $d = 10$, the multilayer swelling capability decreases. This is obvious for the lines corresponding to Barex-SEBS and PVDF-VHB multilayers; however, the PVDF-SEBS film does not show exactly the same trend. The reason for that inconsistency is the nonlinear dependence of the swelling amplitude on the thickness ratio d. This dependence is separately shown in Figure 4 for the PVDF-SEBS film. Both the swelling potential at $V = -V_0/2$ and squeezing potential at $V = V_0/2$ show a maximum and minimum, respectively. Dashed line in the figure corresponds to the squeezing of a single SEBS layer of a thickness L.

We compare the strains of the multilayer films and single layer elastomers for fields up to $E = 50$ MV/m in Figure 5. It is evident that only the PVDF-VHB film has the greatest shrinking strain, which is about 100% at $\sigma_b = 0.01$ C/m^2, and about 200% at $\sigma_b = 0.02$ C/m^2. Also, all multilayer membranes show higher strains compared to the single layer elastomers. For example, the PVDF-VHB film is more than eight times effective than its VHB single layer counterpart, and the Barex-SEBS film is about 16 times effective than its SEBS single layer counterpart when the multilayer films are charged up to $\sigma_b = 0.02$ C/m^2.

Figure 6, where the strain Σ is plotted for different interface charges σ_b, shows that higher swellings can be achieved in strongly charged films. However, in reality, there is an upper limit for how much charge can be put on the interface. This limit depends on the Bjerrum length λ_B of the electron at an interface, which is about $\lambda_B = 6$ nm for a medium with

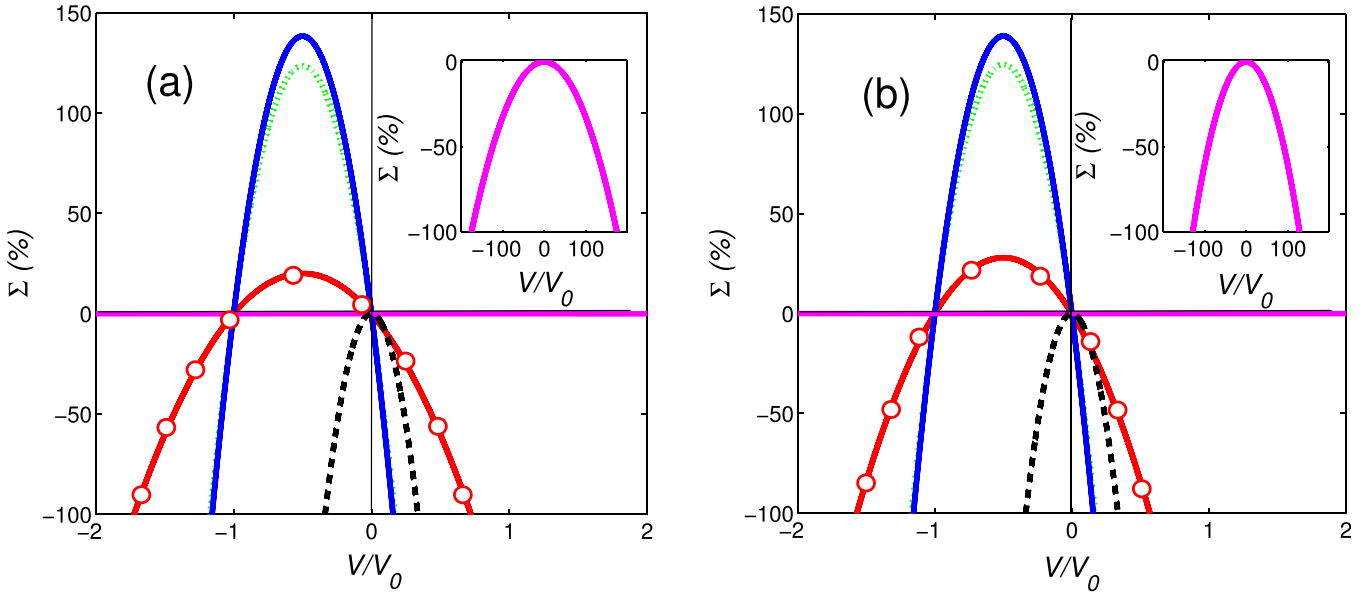

FIG. 3. Calculated strain Σ from Eq. (15) as a function of applied voltage V for $n=20$ and $L=5000\,\mu$m films listed in Table II. Line with symbols (red)—PVDF-SEBS film, dotted line (green)—PVDF-VHB film, full line (blue)—Barex-SEBS film, dashed line (black)—SEBS monolayer film. Applied voltage V is scaled by V_0, and the interface charge density is $\sigma_b = 0.01\,\frac{\mathrm{C}}{\mathrm{m}^2}$. Three thickness ratios $d = d_1/d_2$ are considered: (a) $d=0.1$, (b) $d=1$, and (c) $d=10$. The inset shows the strain of the PZT-VHB film for the voltages in the range $-200V_0 < V < 200V_0$ (in the range of $-2V_0 < V < 2V_0$, accepted in the main figure, the strain is practically zero).

$\epsilon = 10$ at room temperature $T = 300°$C. At distances smaller than λ_B, which corresponds to the surface charge densities $\sigma_b = 0.004$ C/m^2, the electrons strongly repel each other. This surface density limit can be increased if sufficient ion trapping centers are generated at the interfaces. In our study, we will consider a surface charge density $\sigma_b = 0.01$ C/m^2 as being an optimal value for the multilayers.

In Figure 7, we analyze the dependence of g_{33}^R on the elastic and dielectric constants of the layers. This analysis is helpful for locating the domains of the (ϵ, Y) plane

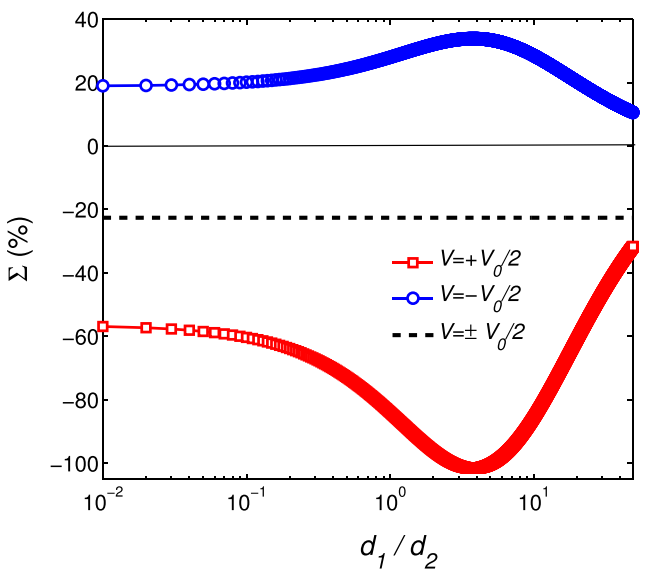

FIG. 4. Calculated strain $\Sigma =$ from Eq. (15) as a function of d_1/d_2 for a PVDF-SEBS multilayer with $n=20$, $L=0.5$ cm, and $\sigma_b = 0.01\,\frac{\mathrm{C}}{\mathrm{m}^2}$. Swelling (line with squares, blue) and shrinking (line with circles, red) branches of the strain are for $V=-V_0/2$ and $V=V_0/2$, respectively. Dashed line (black) is for a SEBS monolayer of the same thickness L.

$(\epsilon = \epsilon_1/\epsilon_2$, and $Y = Y_1/Y_2)$ where maximal swelling or shrinking is expected. We change ϵ between 1 and 20, and Y between 1 and 2000. We note that for $\epsilon \gg 20$, our linear theory predicts unrealistically strong membrane swellings.

Multilayer actuation under the shrinking and swelling voltages, $V = V_0/2$ and $V = -V_0/2$, is separately shown in Figure 7 on the left and right columns, respectively. White lines on the 3D surfaces are for zero multilayer strains. For the convenience of the data presentation, we plot $-g_{33}^R$ instead of g_{33}^R, therefore negative values of $-g_{33}^R$ in Figure 7 correspond to a film shrinking, and positive values of $-g_{33}^R$ correspond to a film swelling. The strength of g_{33}^R, except for using a z-direction color mapping, is additionally visualized by contouring isolines separated from each other by two units. The first pink line above the white line corresponds to $-g_{33}^R = 2$, and the first line below the white line corresponds to $-g_{33}^R = -2$. 3D g_{33}^R surfaces are calculated for three different thickness ratios $d = 0.1$, 1, and 10. For a positive V and $d=0.1$, see the top left picture in Figure 7, the film always shrinks, because the main role here is played by the elastomer layer. For $d=1$ and low Y, the coefficient $-g_{33}^R$ starts to show an upturn, which consequently develops to a strong swelling for $d=10$ in accordance with Eq. (12).

The case of negative voltage $V = -V_0/2$ is very interesting. Here, a strong swelling is seen for all Y values and $\epsilon < 10$ for $d=0.1$ and $d=1$. Comparing these two cases, we see that as the volume fraction of the material I increases, the film's swelling strength decreases nearly twice. A further increase in d, see the case $d=10$ in Figure 7, the $-g_{33}^R$ coefficient decreases again in the region $\epsilon < 10$ and almost for all values of Y. However, in the region $Y < 10$ and $\epsilon > 15$, a strong and narrow swelling strip develops. There are two interesting facts associated with this behavior. First, in this area, previous thickness factors showed weak shrinking.

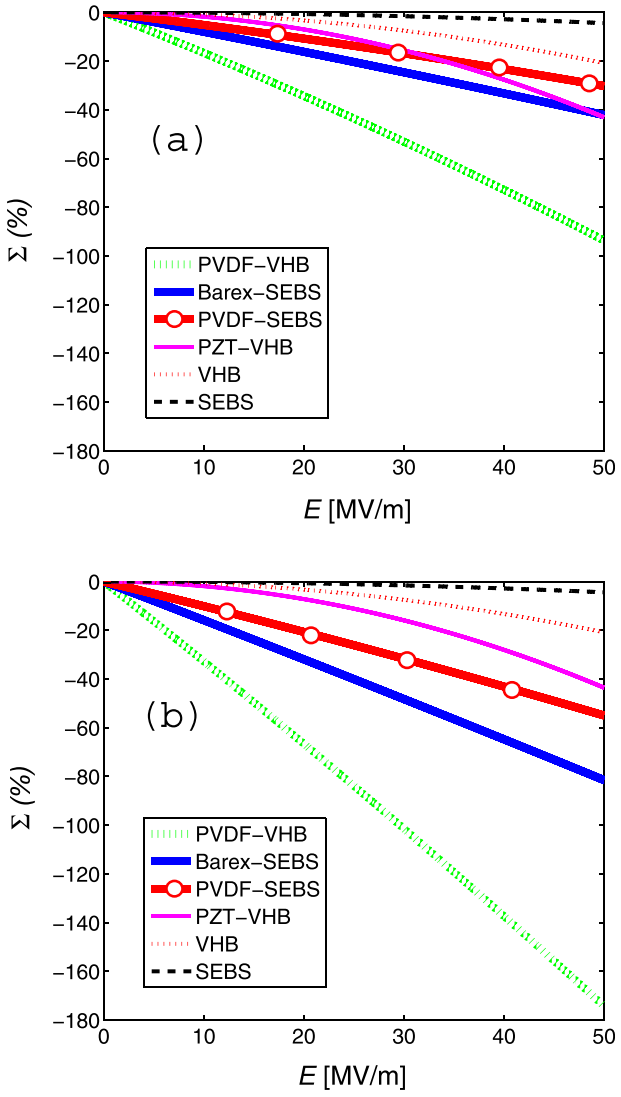

FIG. 5. Calculated strain Σ from Eq. (15) as a function of applied voltage V for $n = 20$ and $L = 5000\,\mu$m films listed in Table II. Dotted line (green)—PVDF-VHB film, full line (blue)—Barex-SEBS film, line with symbols (red)—PVDF-SEBS film, thin full line (pink)—PZT-VHB film, thin dotted line (red)—VHB monolayer film, thin dashed line (black)—SEBS monolayer film. The interface charge density is (a) $\sigma_b = 0.01\,\frac{\mathrm{C}}{\mathrm{m}^2}$ and (b) $\sigma_b = 0.02\,\frac{\mathrm{C}}{\mathrm{m}^2}$. The thickness ratio is $d = d_1/d_2 = 1$. Note that only the shrinking strain $\Sigma < 0$ is shown, which corresponds to the applied voltage $V > 0$.

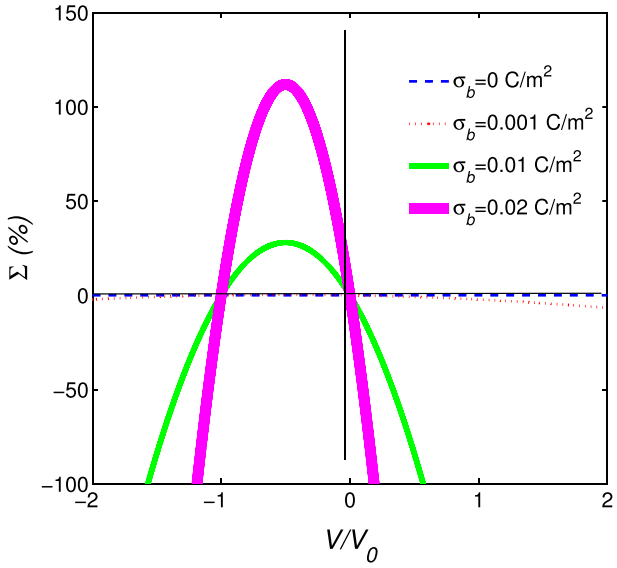

FIG. 6. Calculated strain Σ from Eq. (15) as a function of applied voltage V/V_0 for different interface charge densities σ_b. Dashed line (blue)—$\sigma_b = 0\,\mathrm{C/m^2}$, dotted line (red)—$\sigma_b = 0.001\,\mathrm{C/m^2}$, thin line (green)—$\sigma_b = 0.01\,\mathrm{C/m^2}$, thick line (pink)—$\sigma_b = 0.02\,\mathrm{C/m^2}$. Other parameters: PVDF-SEBS multilayer with $d_1/d_2 = 10$, $n = 20$, and $L = 0.5$ cm.

Second, under a positive voltage, this area also showed a strong swelling. Thus, we conclude that the best candidate for a multilayer film with $d \leq 1$, which strongly shrinks under a squeezing potential $V = V_0/2$, and strongly expands under a swelling potential $V = -V_0/2$ is a film with $Y_1 \approx 10Y_2$, and $\epsilon_1 < 10\epsilon_2$. Also, the best candidate for a multilayer which always swells regardless the polarity of the applied voltage is a film with $d > 1$, $Y < 10$, and $\epsilon > 15$.

The case $d = 10$ has another unexpected feature, such as it has two zero g_{33}^R lines for negative V. The consequences of this are elaborated in Figure 8, where a projection of $-g_{33}^R$ on the (ϵ, Y) plane is shown for $d = 10$ and for six different values of V: $V = \pm V_0/4, \pm V_0/2, \pm V_0$. It is evident that the change of the potential from $V_0/4$ to V_0 on the left column has only a quantitative impact on the film actuation: as the amplitude of the voltage increases, both the squeezing and swelling strengths of the film weaken. On the other hand, when V is changed from $-V_0/4$ to $-V_0$ on the right column of the figure, besides of the quantitative changes we also observe strong qualitative differences. First, at $V = -V_0/4$, in comparison with the case of $V = V_o/4$, see the first row of Figure 8, the swelling and shrinking regions flip their places. Second, the two zero lines at $V = -V_0/2$ and $V = -V_0$ divide the coordinate space into four distinct regions. An imaginary vertical line going from $\epsilon = 1$ to $\epsilon = 20$, and along the fixed $Y = 10^2$ line will pass from a swelling area to a shrinking area. However, if we follow a horizontal line with $Y = 5$ and go along it from $\epsilon = 1$ to $\epsilon = 20$, the result will be opposite: we will pass from a shrinking area to a swelling area. In other words, the results of Figures 7 and 8 can serve as a powerful guide for manufacturing composite material with better and tailored properties. In experiments, a manipulation of the multilayer elastic and dielectric parameters can be achieved by using dopants and/or impregnation of the material with different fillers.

In Figure 9, we plot the relative piezoelectric coefficient d_{33}^R as a function of ϵ and Y. For positive voltages V, see the left column on Figure 9, the value of $\Delta\sigma_s$ for the multilayer is always higher than its corresponding value for a single layer. However, this behavior depends strongly on the relative thickness parameter d. Whereas for $d = 0.1$, a big change in the value of σ_s takes place at low ϵ values, for $d \geq 1$, more than 10 times stronger changes of σ_s are expected at large ϵ values. In other words, the layer thicknesses in a multilayer should be coupled to their dielectric constants for getting better sensory responses for the composite films. The swelling branch of $-d_{33}^R$ at negative voltages V, however, has practically no qualitative dependence on d and shows both negative and positive regions. A positive $-d_{33}^R$ is an indication of the fact that the surface charge σ_s will decrease (increase)

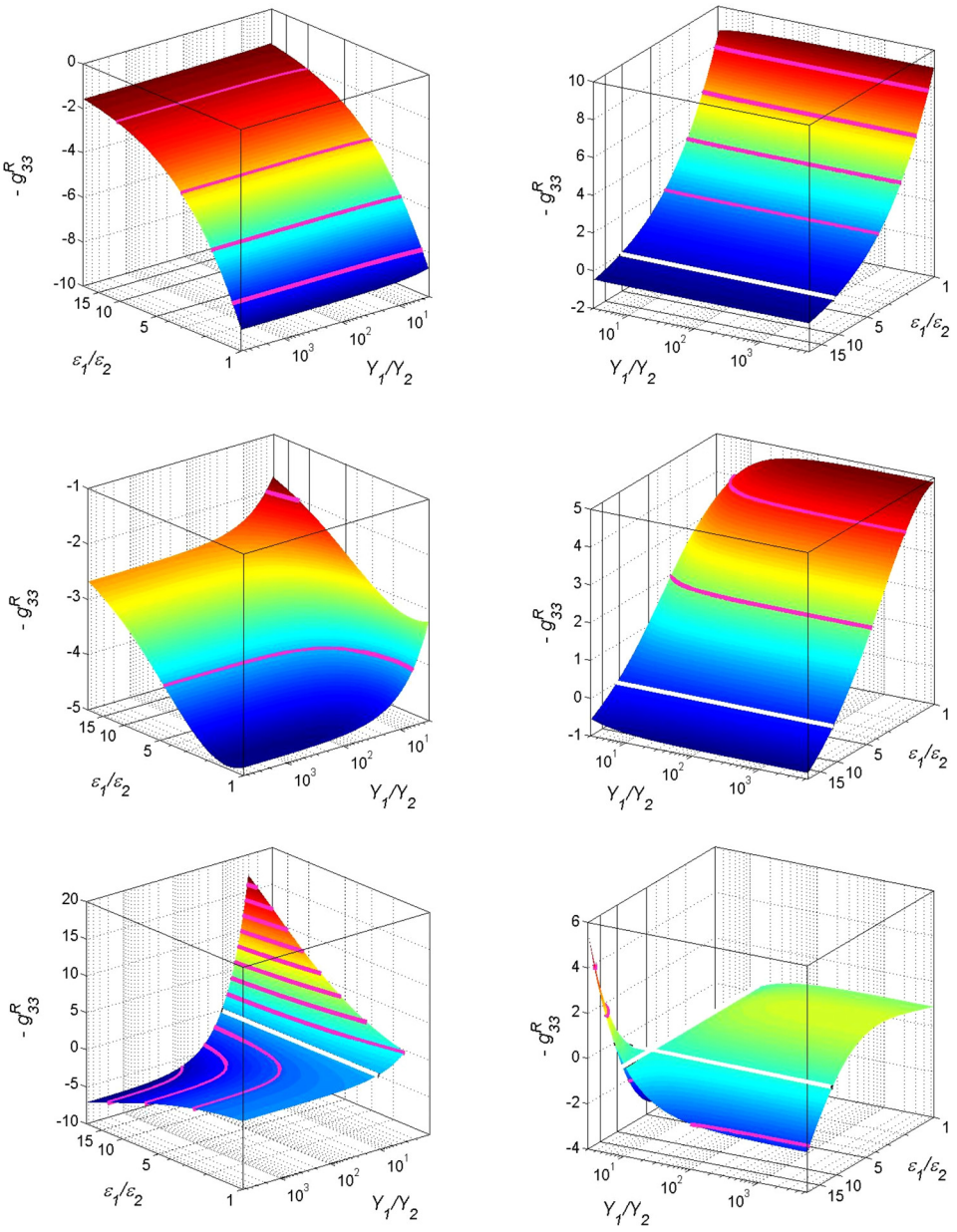

FIG. 7. Relative coefficient $-g^R_{33}$ from Eq. (18) as a function of ϵ_1/ϵ_2 and Y_1/Y_2 for multilayer films for $n=20$, $L=0.5$ cm, and $\sigma_b = 0.01$ C/m^2. As a single layer, a SEBS elastomer with a thickness L is used. White line corresponds to $g^R_{33}=0$, and the set of pink lines above (below) the white line corresponds to $-g^R_{33}$ isolines separated by two units from each other. From top to bottom, $d_1/d_2 = 0.1, 1, 10$. Left column, a squeezing potential $V = V_0/2$, right column, a swelling potential $V = -V_0/2$. The value of V_0 is given by Eq. (7) in the text. Positive (negative) $-g^R_{33}$ means a swelling (shrinking) of the film. Note the use of logarithmic scale in horizontal dimensions for all plots. Also, the x and y axes in the right column pictures are swapped 90° for getting the best view of 3D surfaces.

when the multilayer thickness is shrinking (expanding) under the applied pressure P. We note that this trend cannot be observed in single layer elastomers. In conclusion, comparing the pictures for positive and negative voltages V in Figure 9 for $d \geq 1$, we see that a better candidate for a film which, when mechanically deformed under the applied pressure P, strongly increases its surface charge at $V>0$, and strongly decreases its surface charge at $V<0$ is a film with $\epsilon_1 > 10\epsilon_2$, and practically with all possible values of Y. Note that this conclusion is valid for a moderate value of the interface charge σ_b.

Combining the analyzes of the Figures 7–9, we conclude that a charged multilayer has a versatile response which can be utilized for various sensor applications.

A. Lifting a mass

We now estimate how much weight M can be lifted by a deformed multilayer under an applied voltage V. For this purpose, we calculate the pressure on the film surface resulting from the voltage induced strain Σ,

$$P_s = Y_c\ \Sigma(V). \tag{31}$$

Here, Y_c is the elastic modulus of the composite and $\Sigma(V)$ is given by Eqs. (11) and (15). For finding the parameter Y_c, we take into account the fact that the pressure P_s is the same for all layers *1* and *2*, therefore,

$$P_s = \frac{\Delta d_i}{d_i} Y_i. \tag{32}$$

Then, Eq. (31) can be rewritten as

$$\frac{1}{Y_c} = \frac{nd_1}{L}\frac{1}{Y_1} + \frac{(n-1)d_2}{L}\frac{1}{Y_2}. \tag{33}$$

Finally, the composite elastic modulus is

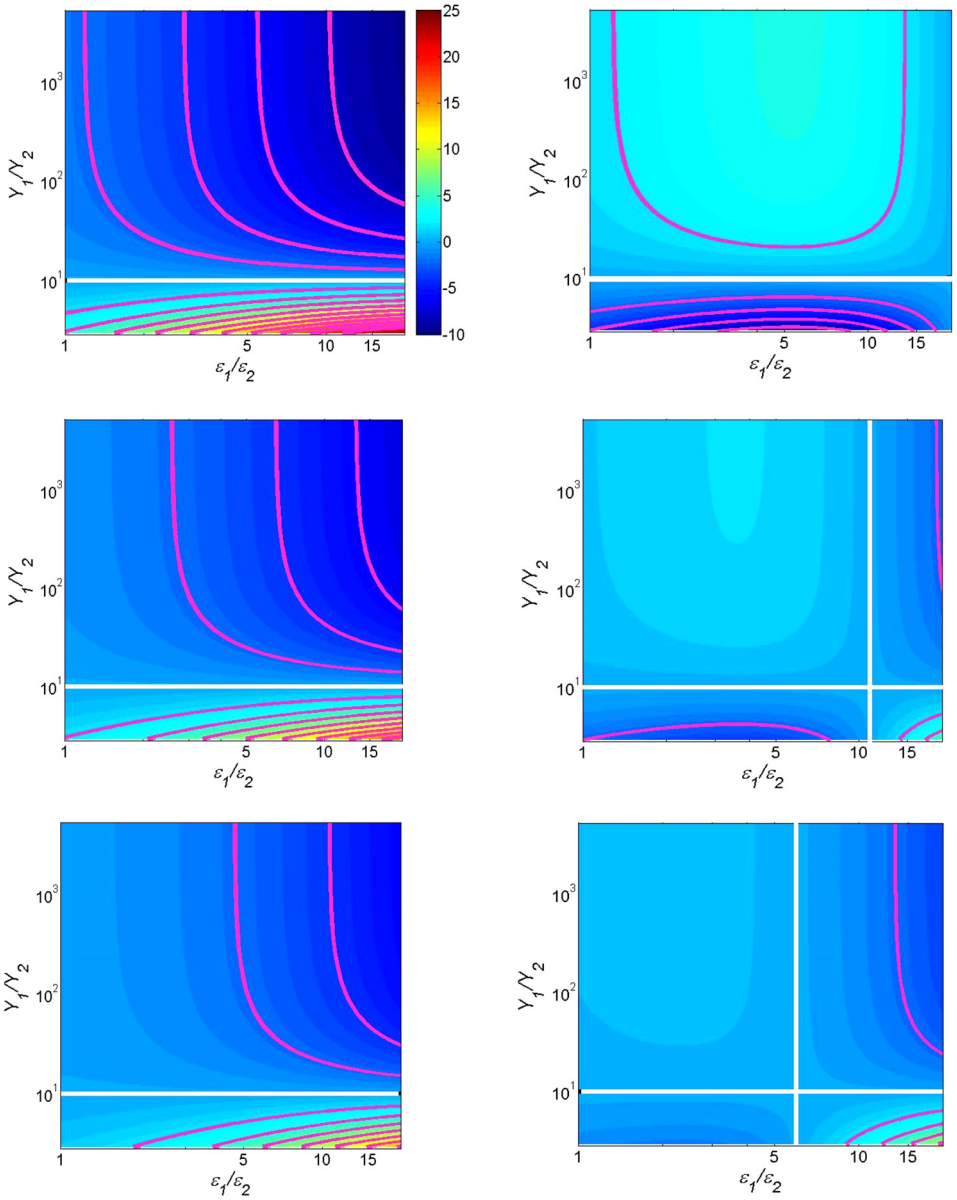

FIG. 8. Top view of the relative coefficient $-g_{33}^R$ from Eq. (18) as a function of ϵ_1/ϵ_2 and Y_1/Y_2 for multilayer films with $n=20$, $L=0.5$ cm, and $\sigma_b = 0.01$ C/m^2. As a single layer, a SEBS elastomer with the same thickness L is considered. White line corresponds to $g_{33}^R = 0$, and the set of pink lines corresponds to $-g_{33}^R$ isolines separated by two units from each other. Left column, from top to bottom: $V = V_0/4$, $V = V_0/2$, $V = V_0$. Right column, from top to bottom: $V = -V_0/4$, $V = -V_0/2$, $V = -V_0$. A color map with dark blue color for $-g_{33}^R = -10$ and a red color for $-g_{33}^R = 25$ is used in all plots. A color map bar is shown next to the top left picture.

$$Y_c = \frac{Y_1 Y_2}{\eta_1 Y_2 + \eta_2 Y_1}, \tag{34}$$

where η_i is the volume fraction of the material i, and $\sum_i \eta_i = 1$. Once the pressure P given by Eq. (31) is known, the value of the lifted mass M can be determined as

$$M = \frac{P_s}{gS}, \tag{35}$$

where S is a surface area of the film, g is the gravity acceleration constant. The dependence of M on the voltage V and on the multilayer strain Σ is shown in Figure 10, where a solid thick line corresponds to a multilayer, and a dashed thin line corresponds to a single layer. Here, two points have to be highlighted. First, whereas the mass lifting of a single layer film is based on its shrinking deformation under the applied V with no dependence on the latter's polarity, the lifting capability of the multilayer is based on its shrinking under a positive V and on its swelling under a negative V. Second, a charged multilayer can lift at least four times more mass than a single layer film does. This is evident from the gradient coloring used in Figure 10: The tips of the dashed line are red, which corresponds to a lifted mass $M \approx 15$ kg, whereas the highest tip of the solid line, which is dark pink, corresponds to $M \approx 60$ kg. Additional inspection of the Figure 10 also reveals that the multilayer shrinking is more powerful than its swelling. The effectiveness of the membrane lifting can be further boosted if the multilayer parameters ϵ, Y, and d are optimized in accordance with the results of Figures 8 and 9.

VII. CONCLUSION

Multilayer films have a great potential for being used as actuators with both swelling and shrinking capabilities. We showed that a charged multilayer has a swelling window $-V_0 < V < 0$ with a maximal swelling at $V = -V_0/2$. For all other voltages V, the multilayer shrinks like a single layer film. At the swelling $V = -V_0/2$ and squeezing $V = V_0/2$

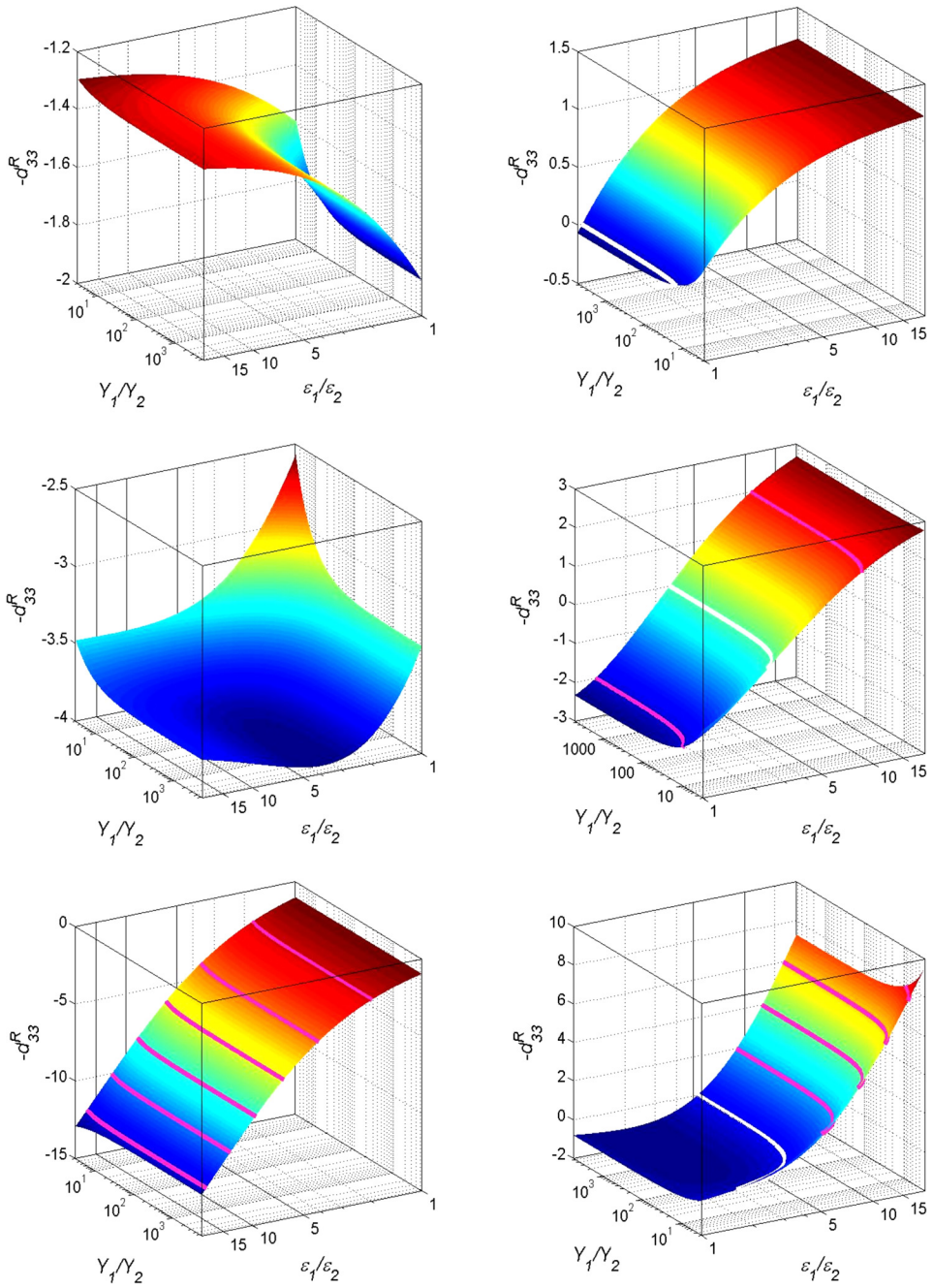

FIG. 9. Relative coefficient $-d_{33}^R$ from Eq. (27) as a function of ϵ_1/ϵ_2 and Y_1/Y_2 for multilayer films with $n=20$, $L=0.5\,\text{cm}$, and $\sigma_b=0.01\,\text{C/m}^2$. As a single layer, a SEBS elastomer with thickness L is considered. White line corresponds to $d_{33}^R=0$, and a set of pink lines above (below) the white line correspond to $-d_{33}^R$ isolines separated by two units from each other. From top to bottom, $d_1/d_2=0.1, 1, 10$. Left column, a squeezing potential $V=0.5\text{MV}$, right column, a swelling potential $V=-0.5$ MV. Note the use of logarithmic scale in horizontal dimensions for all plots.

voltages, the film deformation has a nonlinear dependence on the ratio $d=d_1/d_2$ showing a maximum and minimum, respectively.

We found that a best candidate for a multilayer film with $d\leq 1$, which strongly shrinks under a squeezing potential $V=V_0/2$, and strongly expands under a swelling potential $V=-V_0/2$ is a film with $Y_1\approx 10Y_2$ and $\epsilon_1<10\epsilon_2$. Also, a best candidate for a multilayer which always swells regardless the polarity of the applied voltage is a film with $d>1$, $Y<10$, and $\epsilon>15$. Note that no single layer film can swell under any applied voltage. We show that when $d>1$ and $V<V_0$, two zero g_{33}^R lines divide the (ϵ, Y) plane into four distinct regions. Then, depending on which of the film parameters is changed by the addition of dopants, ϵ or Y, it is possible to swell the initially shrunken film, or to shrink the initially swollen film.

Our analysis of the coefficient d_{33}^R reveals that the change of σ_s strongly depends on the relative thickness parameter d. The larger change in σ_s happens at low ϵ for small d, and at high ϵ for large d. In other words, the layer thicknesses in a multilayer should be coupled to their dielectric constants for getting better sensory responses for the composite films. Our results show that a better candidate for a film which, when mechanically deformed, strongly increases its surface charge at $V>0$, and strongly decreases its surface charge at $V<0$ is a film with $\epsilon_1>10\epsilon_2$, and practically with all possible values of Y.

We demonstrated that a multilayer shrinking has more power to lift a weight compared to a membrane swelling. Also, the multilayer deformation is energetically stronger than a single layer deformation. For example, a charged PVDF-SEBS film can lift at least four times more weight than a single layer SEBS film.

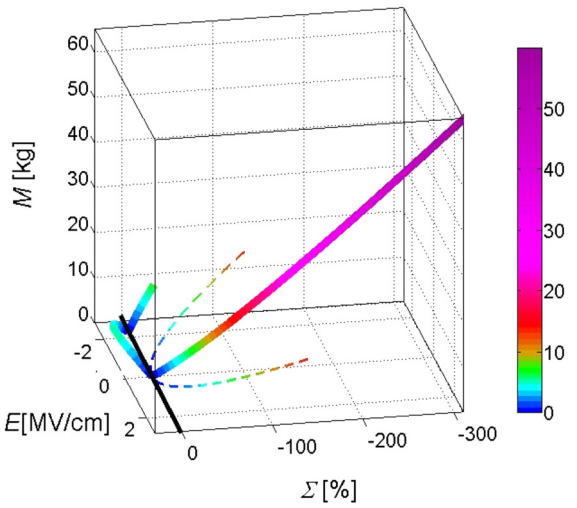

FIG. 10. Lifted mass M in kg as a function of the applied voltage V and the resulting strain Σ in the PVDF-SEBS multilayer with $n=20$, $d_1/d_2=1$, $L=0.5$ cm, $\sigma_s=0.01$ C/m^2, and an area $S=1$ cm^2. Thick full line—a multilayer, thin dashed line—a single SEBS layer. The color map corresponds to the value of the lifted mass.

When it comes to the role of the number of layers in the multilayer, our results show that the parameter n has a dual role in the multilayer response. On one hand, the mass lifting capacity of the multilayer, as shown in Figure 11, decreases as n increases. On the other hand, more layering stabilizes the piezoelectric response of films. In Figure 12, we show g_{33}^R coefficients for two different multilayers with $n=2$ (upper picture) and $n=40$ (lower picture), respectively. It is evident that the case $n=40$ has an overall better shrinking response, namely, the low ϵ and low Y regions of $-g_{33}^R$ are stabilized. Also, thinner layers are better suited for avoiding charge migration problems in stacked layers under external fields.[23]

In the framework of current analytical theory, we omitted the change of the film's lateral x and y directions for the sake of getting tractable analytical results. A full consideration of the membrane actuation[7] must address the mismatch between the lateral stretching of the layers and associated with it the change of the interface charge densities. A modified theory should also take into account the generation of permanent dipoles and charges in the piezolayer caused by the applied voltages and pressures. Another issue concerns huge strains and associates with it the change in ϵ and Y of the multilayer. Also, high strains cannot appear instantly, and thus the theory should introduce a separation of the stress and time functions.[7]

The results reported here allow us to propose other than simple slab geometries for exploring the dependence of Σ on the multilayer parameters. For example, it is possible to create a film which differently responds to the applied field

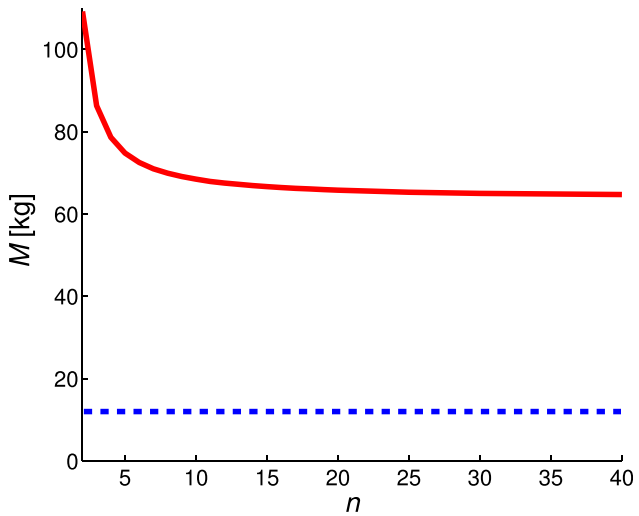

FIG. 11. Dependence of the lifted mass M on the number of layers n. Other system parameters are PVDF-SEBS multilayer with $d_1/d_2=1$, $L=0.5$ cm, $\sigma_s=0.01$ C/m^2, $V/L=2$MV, and $S=1$ cm^2. Full line (red) is for a multilayer, dashed line (blue) is for a single layer.

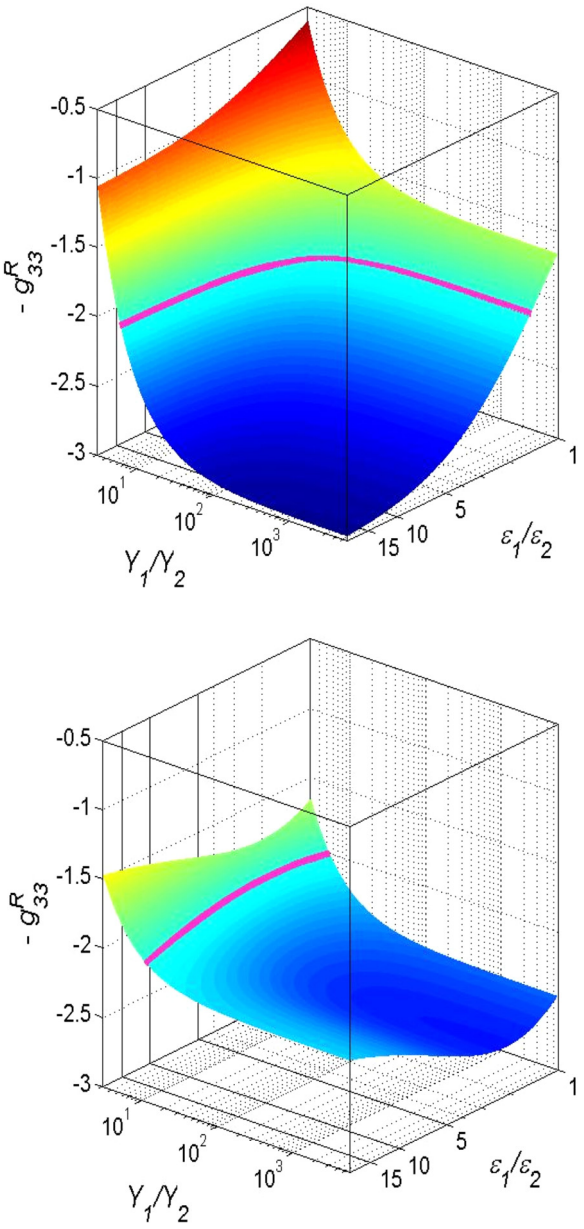

FIG. 12. Relative coefficient $-g_{33}^R$ from Eq. (18) as a function of ϵ_1/ϵ_2 and Y_1/Y_2 for multilayer films with $L=0.5$ cm, $\sigma_b=0.01$ C/m^2, $d_1/d_2=1$, and $V=V_0/2$. As a single layer, a SEBS elastomer with thickness L is considered. Pink line corresponds to the -2 isoline of $-g_{33}^R$. Upper picture: $n=2$, lower picture: $n=40$. Note the use of logarithmic scale in horizontal dimensions for all plots.

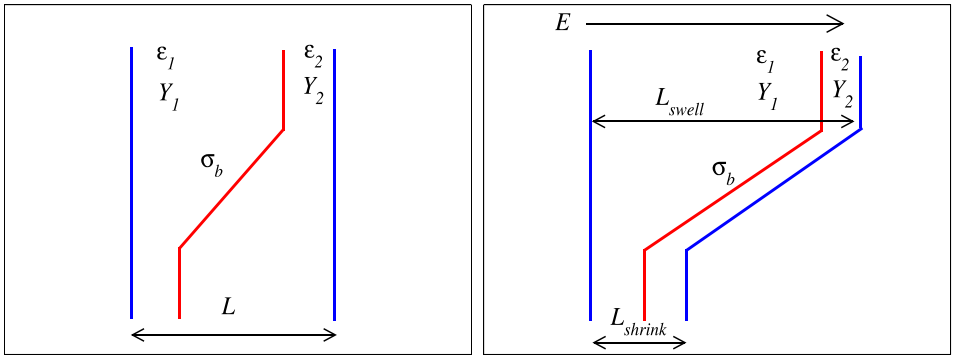

FIG. 13. Schematic illustration of the charged bilayer response to the applied field E. The layer thickness is not uniform along the film direction. The deformation can be manipulated by changing the interface charge density σ_b and the initial layer thicknesses.

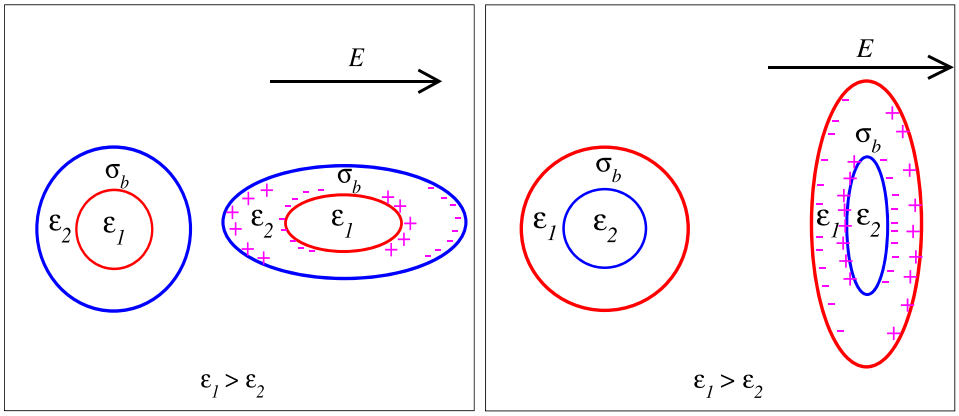

FIG. 14. Schematic illustration of the bilayer core-shell colloid particle's response to the external field E. The direction of particle elongation depends on the core-shell permittivity ratio ϵ_1/ϵ_2. The deformation can be manipulated by changing the interface charge density σ_b and the initial layer thicknesses.

through the variation of d_1/d_2 along the interface. In Figure 13, we show a specific case when the upper part of the film swells, whereas the bottom part of the film shrinks. Such film can be used as a building block for more complicated structures, such as for creating a gating architecture, or developing a caging geometry. Another interesting application might be core-shell colloidal particles which can be used for shape-controlled colloidal interactions.[32] As shown schematically in Figure 14, such system, depending on where a high ϵ material is used, in the core or in the shell, can either elongate or shrink along the applied voltage.

It is also possible to build smart structures from the multilayer blocks A and B which differently respond to the applied field, see Figure 15. For example, a chained A-B-A-B-A structure, when put on a surface with a vanishing friction coefficient in one direction, will move in that direction by converting the energy of the applied ac-field $V = \frac{V_0}{2} e^{i\omega t}$ into a kinetic energy.

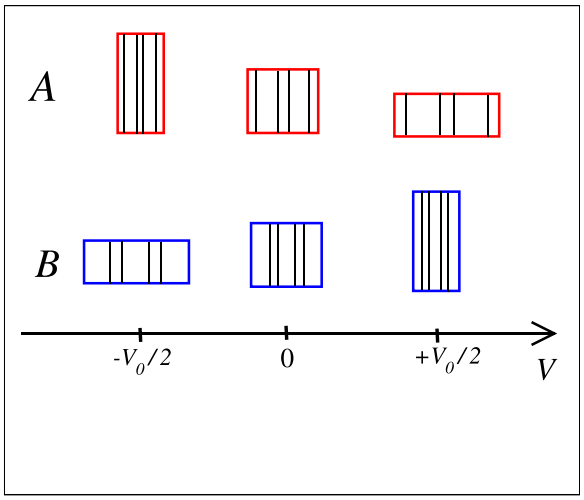

FIG. 15. Schematic illustration of the multilayer blocks A and B which differently respond to the applied voltage V. The relative thickness parameter d in block A is smaller than its value in block B. A consecutive connection of these blocks into a $A-B-A-B-A$ chain can turn the energy of the applied ac field into the kinetic energy of the chain movement.

ACKNOWLEDGMENTS

H.L. thanks the Deutsche Forschungsgemeinschaft for support of the work through the SPP 1681 on magnetic hybrid materials.

L.Z. acknowledges support by National Science Foundation through the Science and Technology Center for Layered Polymeric System (CLiPS) under Grant No. DMR-0423914 and Department of Defense (W911NF-13-1-0153). E.A. thanks Philip Taylor from Physics Department of CWRU for interesting and fruitful discussions.

APPENDIX A: FILM DEFORMATION UNDER CONSTANT VOLUME CONDITION

Constant volume condition for a film with initial dimensions L and S and final dimensions $L + \Delta L$ and $S - \Delta S$ under a decompression field is written as $LS = (L + \Delta L)(S - \Delta S)$. The energy density stored in the film is defined as

$$\eta = \frac{1}{2} DE = \frac{\sigma^2}{2\epsilon_0 \epsilon} = \frac{q^2}{2\epsilon_0 \epsilon S^2}, \tag{A1}$$

where D and E are local electric displacement and fields inside the film, $q = \sigma S$ is the total charge on the plates. Total energy stored in the dielectric is

$$U = \eta SL = \frac{q^2 L}{2\epsilon_0 \epsilon S}. \tag{A2}$$

Deformations ΔL and ΔS lead to the change in the stored energy

$$\Delta U = \frac{\partial U}{\partial L}\Delta L + \frac{\partial U}{\partial S}\Delta S. \tag{A3}$$

Here, the partial derivatives of the stored energy are defined from Eq. (A2)

$$\frac{\partial U}{\partial L} = \frac{1}{2}\frac{q^2}{\epsilon_0 \epsilon S}, \quad \frac{\partial U}{\partial S} = -\frac{1}{2}\frac{q^2 L}{\epsilon_0 \epsilon S^2}. \tag{A4}$$

For the cases when the contact area of the dielectric does not change, $\Delta S = 0$, which is valid for an infinite (in the y and z directions) plates, we have

$$\Delta U = \frac{\partial U}{\partial L}\Delta L = F\Delta L, \tag{A5}$$

and thus recover Eq. (B1)

$$F = \frac{\partial U}{\partial L} = \frac{1}{2}\frac{q^2}{\epsilon_0 \epsilon S} = \frac{1}{2}\frac{\sigma^2}{\epsilon_0 \epsilon} S. \tag{A6}$$

For a finite size plate

$$\Delta S = \frac{S}{L + \Delta L}\Delta L, \tag{A7}$$

and thus, using Eqs. (A3), (A4), and (A7) we get

$$\Delta U = \frac{1}{2}\frac{q^2}{\epsilon_0 \epsilon S}\left(1 + \frac{L}{L + \Delta L}\right)\Delta L = \frac{1}{2}\frac{q^2}{\epsilon_0 \epsilon S}\left(2 - \frac{\Delta S}{S}\right)\Delta L. \tag{A8}$$

Taking into account that in many cases, we can omit the second term $\frac{\Delta S}{S} \ll 1$ on the right side of Eq. (A8), we end up with

$$\Delta U = \frac{q^2}{\epsilon_0 \epsilon S}\Delta L \tag{A9}$$

or

$$F = \frac{q^2}{\epsilon_0 \epsilon S} = \frac{\sigma^2}{\epsilon_0 \epsilon} S. \tag{A10}$$

The difference between Eqs. (A10) and (A6) is the coefficient 1/2.

APPENDIX B: MAXWELLIAN STRAIN OF SINGLE LAYER FILMS

Interaction force between charged electrodes with a dielectric between them is

$$F/S = \epsilon_0 \epsilon E^2 = \sigma^2/(\epsilon_0 \epsilon), \tag{B1}$$

where surface charge density on the electrodes is $\sigma = \epsilon_o \epsilon E = \epsilon_0 \epsilon V/L$. Under the applied voltage V, the film shrinks by

$$\Delta L = -\frac{FL}{SY}. \tag{B2}$$

Thus, for the strain $\Sigma = \Delta L/L$ we get

$$\Sigma = -\frac{F}{SY} = -\frac{\sigma^2}{\epsilon_0 \epsilon Y} = -\frac{\epsilon_0 \epsilon V^2}{L^2 Y}. \tag{B3}$$

The negative sign of the strain means a shrinking of the film under the Maxwellian stress.

[1] R. E. Newnham, "Molecular mechanisms in smart materials," Mater. Res. Soc. Bull. **22**, 20 (1997).
[2] L. S. McCarty and G. M. Whitesides, "Electrostatic charging due to separation of ions at interfaces: Contact electrification of ionic electrets," Angew. Chem. Int. **47**, 2188 (2008).
[3] P. Brochu and Q. Pei, "Advances in dielectric elastomers for actuators and artificial muscles," Macromol. Rapid. Commun. **31**, 10 (2010).
[4] X. Zhang, G. Sessler, and J. Hillenbrand, "Improvement of piezoelectric coefficient of cellular polypropylene films by repeated expansions," J. Electrostat. **65**, 94 (2007).
[5] J. Hillenbrand and G. M. Sessler, "DC-based ferroelectrets with large piezoelectric d_{33} coefficients," J. Appl. Phys. **103**, 074103 (2008).
[6] J. Hillenbrand and G. M. Sessler, "Verification of a model for the piezoelectric d_{33} coefficient of cellular electret films," J. Appl. Phys. **98**, 064105 (2005).
[7] J. D. Nam, H. R. Choi, J. C. Koo, Y. K. Lee, and K. J. Kim, *Dielectric Elastomers for Artificial Muscles, Electroactive Polymers for Robotic Applications* (Springer, London, 2007), pp. 37–48.
[8] D. L. Henann, S. A. Chester, and K. Bertoldi, "Modeling of dielectric elastomers: Design of actuators and energy harvesting devices," J. Mech. Phys. Solids **61**, 2047–2066 (2013).
[9] S. Chiba, M. Waki, T. Wada, Y. Hirakawa, K. Masuda, and T. Ikoma, "Consistent ocean wave energy harvesting using electroactive polymer (dielectric elastomer) artificial muscle generators," Appl. Energy **104**, 497–502 (2013).
[10] S. Chuba and M. Waki, "Extending applications of dielectric elastomer artificial muscles to wireless communication systems," in *Recent Advances in Wireless Communications and Networks*, edited by J. C. Lin (Intech, 2011), p.435.
[11] Z. Suo, "Theory of dielectric elastomers," Acta Mech. Solida Sin. **23**, 549 (2010).
[12] I. A. Anderson *et al.*, "Multi-functional dielectric elastomer artificial muscles for soft and smart machines," J. Appl. Phys. **112**, 041101 (2012).
[13] T. Mirfakhrai, J. D. W. Madden, and R. H. Baughman, "Polymer artificial muscles," Mater. Today **10**, 30–38 (2007).
[14] Kh. S. Ramadan, D. Sameoto, and S. Evoy, Smart Mater. Struct. **23**, 033001 (2014).
[15] Q. Xunlin, X. Zhongfu, and W. Feipeng, "Piezoelectricity of single- and multi-layer cellular polypropylene film electrets," Front. Mater. Sci. China **1**, 72 (2007).
[16] C. R. Bowen and V. Yu. Topolov, "Piezoelectric sensitivity of PbTiOs based ceramic/polymer composites with.0-3 and 3-3 connectivity," Acta Mater. **51**, 4965 (2003).
[17] A. Aliev *et al.*, "Giant-stroke, superelastic carbon nanotube aerogel muscles," Science **323**, 1575 (2009).
[18] M. A. Wolak, M. J. Pan, A. Wan, J. S. Shirk, M. Mackey, A. Hiltner, E. Baer, and L. Flandin, "Dielectric response of structured multilayered polymer films fabricated by forced assembly," Appl. Phys. Lett. **92**, 113301 (2008).
[19] S. Zhukov and H. von Seggern, "Polarization hysteresis and piezoelectricity in open-porous fluoropolymer sandwiches," J. Appl. Phys. **102**, 044109 (2007).
[20] J. Hillenbrand and G. M. Sessler, "Piezoelectricity in cellular electret films," IEEE Trans. Dielec. Electr. Insul. **7**, 537 (2000).

[21]V. Leonov, C. Van Hoof, M. Goedbloed, and R. van Schaijk, "Charge injection and storage in single-layer and multilayer electrets based on SiO_2 and Si_3N_4," IEEE Trans. Dielectr. Electr. Insul. **19**, 1253 (2012).
[22]E. Tuncer, M. Wegener, and R. Gerhard-Multhaup, "Modeling electromechanical properties of layered electrets: Application of the finite-element method," J. Electrostat. **63**, 21 (2005).
[23]M. Mackey, D. E. Schuele, L. Zhu, L. Flandin, M. A. Wolak, J. S. Shirk, A. Hiltner, and E. Baer, "Reduction of dielectric hysteresis in multilayered films via nanoconfinement," Macromolecules **45**, 1954 (2012).
[24]R. E. Newnham, D. P. Skinner, and L. E. Cross, "Connectivity and piezoelectric-pyroelectric composites," Mater. Res. Bull. **13**, 525 (1978).
[25]D. A. van den Ende, B. F. Bory, W. A. Groen, and A. van der Zwaag, "Improving the d_{33} and g_{33} properties of 0-3 piezoelectric composites by dielectrophoresis," J. Appl. Phys. **107**, 024107 (2010).
[26]H. Vandeparre, S. Gabriele, F. Brau, C. Gay, K. K. Parkerc, and P. Damman, "Hierarchical wrinkling patterns," Soft Matter **6**, 5751 (2010).
[27]A. T. Conn and J. Rossiter, "Harnessing electromechanical membrane wrinkling for actuation," Appl. Phys. Lett. **101**, 171906 (2012).
[28]H. C. Chan and O. Foo, "Buckling of multi-layer sandwich plates by the finite strip method," Int. J. Mech. Sci. **19**, 447 (1977).
[29]G. M. Sessler and J. E. West, "Self-biased condenser microphone with high capacitance," J. Acoust. Soc. Am. **34**, 1787 (1962).
[30]R. Kacprzyk, A. Dobrucki, and J. B. Gajewski, "Double-layer electret transducer," J. Electrostat. **39**, 33 (1997).
[31]R. Kacprzyk and A. Kisiel, "Piezo-electric properties of polypropylene laminates with a non-woven layer," J. Electrostat. **71**, 400 (2013).
[32]C. P. Lapointe, T. G. Mason, and I. I. Smalyukh, "Shape-controlled colloidal interactions in nematic crystals," Science **326**, 1083 (2009).